Probing Slow Time Scale Dynamics at Methyl-Containing Side Chains in Proteins by Relaxation Dispersion NMR Measurements: Application to Methionine Residues in a Cavity Mutant of T4 Lysozyme

Nikolai R. Skrynnikov,[†] Frans A. A. Mulder,[†] Bin Hon,[‡] Frederick W. Dahlquist,[‡] and Lewis E. Kay*,[†]

Contribution from the Protein Engineering Network Centres of Excellence and Departments of Medical Genetics, Biochemistry and Chemistry, University of Toronto, Toronto, Ontario, M5S 1A8 Canada, and Institute of Molecular Biology and Department of Chemistry, University of Oregon, Eugene, Oregon 97403

Abstract: A relaxation dispersion-based NMR experiment is presented for the measurement and quantitation of μs–ms dynamic processes at methyl side-chain positions in proteins. The experiment measures the exchange contribution to the ^{13}C line widths of methyl groups using a constant-time CPMG scheme. The effects of cross-correlated spin relaxation between dipole–dipole and dipole–CSA interactions as well as the effects of scalar coupling responsible for mixing of magnetization modes during the course of the experiment have been investigated in detail both theoretically and through simulations. It is shown that the complex relaxation properties of the methyl spin system do not complicate extraction of accurate exchange parameters as long as care is taken to ensure that appropriate magnetization modes are interchanged in the middle of the constant-time CPMG period. An application involving the measurement of relaxation dispersion profiles of methionine residues in a Leu99Ala substitution of T4 lysozyme is presented. All of the methionine residues are sensitive to an exchange event with a rate on the order of 1200 s^{-1} at 20 °C that may be linked to a process in which hydrophobic ligands are able to rapidly bind to the cavity that is present in this mutant.

Introduction

Dynamics play an important role in controlling stability, ligand affinity, catalysis, and the specificity of molecular interactions.[1–3] NMR spectroscopy is particularly well suited to study protein internal dynamics over a wide range of time scales via nuclear spin relaxation.[4–6] In the past decade NMR studies of protein dynamics have focused to a large extent on measurement and interpretation of rapid, ps–ns time scale motions, predominately at backbone positions in the molecule.[4] More recently methodology has been extended to investigate rapid processes in side chains through the use of ^{13}C[7–10] and ^{2}H[11,12] spin relaxation spectroscopy. Comparatively fewer studies have been reported on dynamic events occurring on longer time

scales which are thought to be important in many biological processes. For example, enzyme catalysis and product-release rates[13] in many systems are on the order of 10 to 10^5 s^{-1}, and protein-folding rates[14] fall in the range of 10^{-1} to 10^5 s^{-1}. Protein motions underlying these processes will therefore have time constants in the microsecond-to-millisecond range. Relaxation dispersion experiments have been developed to probe such slow processes at backbone positions in proteins, allowing extraction of populations, chemical shift differences, and the rates of interconversion between states.[15–17] More recently, Ishima and Torchia have developed an experiment for establishing the presence of chemical exchange at side-chain methyl sites in proteins by comparing relaxation rates measured at different effective radio frequency fields using $^{13}CHD_2$ methyls as probes of dynamics.[18] In addition, Mulder et al. have described an approach for quantifying exchange at side-chain Asn and Gln positions by recording relaxation dispersion profiles of $^{15}NH_2$ groups.[19]

We present here an experiment to quantitate exchange

[†] University of Toronto, Toronto.

[‡] University of Oregon.

(1) Frauenfelder, H.; Parak, F.; Young, R. D. *Annu. Rev. Biophys. Biophys. Chem.* **1988**, *17*, 451–479.

(2) Karplus, M.; McCammon, J. A. *Annu. Rev. Biochem.* **1983**, *53*, 263–300.

(3) Alber, T.; Gilbert, W. A.; Ponzi, D. R.; Petsko, G. A. *Ciba Found. Symp.* **1983**, *93*, 4–24.

(4) Palmer, A. G. *Curr. Opin. Struct. Biol.* **1997**, *7*, 732–737.

(5) Kay, L. E. *Nat. Struct. Biol. NMR Suppl.* **1998**, *5*, 513–516.

(6) Ishima, R.; Torchia, D. A. *Nat. Struct. Biol* **2000**, *7*, 740–743.

(7) Henry, G. D.; Weiner, J. H.; Sykes, B. D. *Biochemistry* **1986**, *25*, 590–598.

(8) Nicholson, L. K.; Kay, L. E.; Baldisseri, D. M.; Arango, J.; Young, P. E.; Bax, A.; Torchia, D. A. *Biochemistry* **1992**, *31*, 5253–5263.

(9) Wand, A. J.; Urbauer, J. L.; McEvoy, R. P.; Bieber, R. J. *Biochemistry* **1996**, *35*, 6116–6125.

(10) LeMaster, D. M.; Kushlan, D. M. *J. Am. Chem. Soc.* **1996**, *118*, 9255–9264.

(11) Muhandiram, D. R.; Yamazaki, T.; Sykes, B. D.; Kay, L. E. *J. Am. Chem. Soc.* **1995**, *117*, 11536–11544.

(12) Yang, D.; Mittermaier, A.; Mok, Y. K.; Kay, L. E. *J. Mol. Biol.* **1998**, *276*, 939–954.

(13) Fersht, A. *Enzyme Structure and Mechanism*, 2nd ed.; Freeman & Co.: New York, 1985.

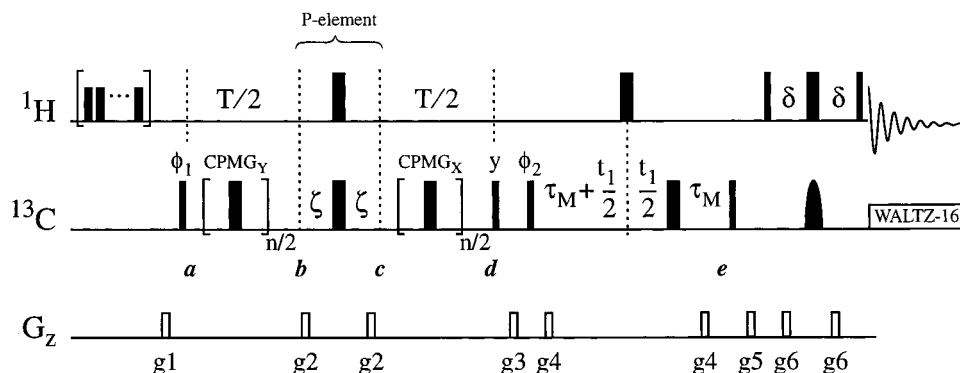(14) Jackson, E. S. *Folding Des.* **1998**, *3*, 81–91.

(15) Akke, M.; Palmer, A. G. *J. Am. Chem. Soc.* **1996**, *118*, 911–912.

(16) Mulder, F. A. A.; van Tilborg, P. J. A.; Kaptein, R.; Boelens, R. *J. Biomol. NMR* **1999**, *13*, 275–288.

(17) Loria, J. P.; Rance, M.; Palmer, A. G. *J. Am. Chem. Soc.* **1998**, *121*, 2331–2332.

(18) Ishima, R.; Louis, J. M.; Torchia, D. A. *J. Am. Chem. Soc.* **1999**, *121*, 11589–11590.

(19) Mulder, F. A. A.; Skrynnikov, N. R.; Hon, B.; Dahlquist, F. W.; Kay, L. E. *J. Am. Chem. Soc.* **2001**, *123*, 967–975.

Figure 1. Pulse scheme used to measure relaxation dispersion profiles of CH_3 groups in ^{13}C-methyl-labeled proteins. All narrow (wide) pulses are applied with flip angles of 90° (180°) along the *x*-axis, unless indicated otherwise. ^1H pulses used for the NOE buildup at the start of the sequence are applied with a 120° flip angle[28] using a 7.5 kHz field at a spacing of 5 ms. All other ^1H pulses use a field of 37 kHz. The ^1H carrier is centered at 2 ppm, until immediately after the final ^{13}C 90° pulse when it is jumped to 4.7 ppm (water). The proton 180° pulses between points *b* and *e* are of the composite variety.[58] All rectangular ^{13}C pulses (centered at 17 ppm) between points *a* and *d* use a field of 5.1 kHz, with the remaining pulses applied using an 18.8 kHz field. The shaped ^{13}C pulse has the RE-BURP profile[59] (2.5 ms at 600 MHz, centered at 15.2 ppm) and is applied to eliminate all $^1H-^{13}C$ correlations that are downfield of 24 ppm in the carbon dimension. (Note that all methionine correlations lie between 15 and 19 ppm for the proteins that we have examined). In cases where spectra of other methyl-containing amino acids are recorded, the bandwidth of the selective RE-BURP pulse would be modified. ^{13}C decoupling is achieved using a 2.5 kHz WALTZ-16 scheme.[60] Each $CPMG_Y$ train is of the form $(\tau - 180_y^\circ - \tau)_{n/2}$, with $T = n(2\tau + pw_C^{180^\circ})$, with $pw_C^{180^\circ}$ the ^{13}C 180° pulse width, and $n/2$ is even. The delays used are: $T = 40$ ms, $\zeta = 1/(4J_{CH}) = 1.8$ ms, $\tau_M = 0.705$ ms, $\delta = 1.8$ ms, where 2δ is the total duration between the final two ^1H 90° pulses. The phase cycle is: $\phi 1 = (x,-x)$; $\phi 2 = 2(x),2(-x)$; rec $= x,2(-x),x$. Quadrature detection in F_1 is achieved using States-TPPI[61] of $\phi 2$. The strengths and durations of the gradients are: $g1 = (1$ ms, 5 G/cm$)$; $g2 = (0.6$ ms, 20 G/cm$)$; $g3 = (0.5$ ms, -15 G/cm$)$; $g4 = (0.1$ ms, 20 G/cm$)$; $g5 = (0.6$ ms, 12 G/cm$)$; $g6 = (0.3$ ms, 12 G/cm$)$.

processes at methyl positions in proteins using relaxation dispersion measurements. Methyl groups are ideally suited for the study of protein dynamics since the three-fold methyl rotation leads to reasonably narrow resonance lines[20] and the correlations in the methyl region of $^{13}C-^1H$ spectra are generally well-resolved even for proteins on the order of 15−20 kDa in molecular mass. A detailed analysis is provided to establish that cross-correlated spin relaxation and scalar-coupled evolution, both of which connect magnetization modes with different relaxation rates, do not complicate extraction of accurate exchange parameters in the methyl spin system using the experimental scheme described below. The methodology is illustrated with an application to the study of ms time scale side-chain dynamics of methionine residues in a buried cavity mutant of T4 lysozyme, L99A, in which a leucine residue is replaced by an alanine.[21,22] This substitution results in the formation of a 150 Å^3 buried cavity in the C-terminal domain of the protein,[23] which binds hydrophobic ligands such as substituted benzenes in rapid order[24] (off rates of 300 and 800 s^{-1} for indole and benzene, respectively, at 20 °C). The present study establishes that all of the methionines in the protein sense a slow exchange process with an average rate of 1190 ± 200 s^{-1} at 20 °C, with those residues in proximity to the cavity affected the most. These motions are likely linked to a process which allows entry and exit of ligands to and from the cavity.

Materials and Methods

Sample Conditions and NMR Measurements. A uniformly $^{15}N/$ ^{13}C-labeled sample of T4 lysozyme containing the following mutations, C54T/C97A/L99A, was prepared as described previously.[25] The sample consisted of 1 mM protein, 50 mM sodium phosphate, 25 mM sodium chloride, pH 5.5. All data sets were recorded at temperatures of 25° and 20 °C on Varian Inova 600 and 800 MHz spectrometers. Assignments of methionine residues were obtained as described in a previous publication.[26]

An $^{15}N/^{13}C$-labeled sample of calmodulin in complex with an unlabeled 26 residue peptide from the C-terminal domain of petunia glutamate decarboxylase was generated as published previously.[27] Sample conditions were: 1.5 mM protein, 100 mM potassium chloride, pH 5.5. Spectra were recorded at 25 °C on a Varian Inova 600 MHz spectrometer.

Relaxation dispersion spectra were recorded using the pulse scheme of Figure 1 with effective B_1 field strengths of 50, 100, 150, 200, 250, 300, 350, 400, 500, 600, 700, 800, 900, and 1000 Hz, with repeats at fields of 150, 500 and 1000 Hz. In addition, a single reference spectrum was obtained with the periods extending from *a* to *b* and *c* to *d* omitted. Each data set was comprised of 128×576 complex points (600 MHz) or 128×768 complex points (800 MHz). (F_1,F_2) spectral widths of 3600, 9000 Hz (600 MHz) or 3600, 12 000 Hz (800 MHz) were employed, corresponding to (t_1,t_2) acquisition times of 35.3 ms, 64 ms. Twelve scans were recorded per FID with a relaxation delay of 1.5 s, giving rise to net acquisition times of 1.3 h/spectrum. The $^1H-^{13}C$ steady-state NOE was developed by applying ^1H 120° pulses at intervals of 5 ms for the duration of the relaxation delay.[28]

Data sets were processed and peak intensities quantitated using the NMRPipe software package.[29] Intensities of correlations in each of the experiments were divided by the corresponding intensities in the reference spectrum to generate effective relaxation rates at each B_1 field. Each profile was fit to (i) a flat line, (ii) the fast-exchange equation,[30] and (iii) the general equation for two-site exchange[31−33] (see eq 3 of Millet et al.[34]). *F*-statistics[35] were computed to establish whether statistically significant improvements to the fits were obtained by the

(20) Kay, L. E.; Bull, T. E.; Nicholson, L. K.; Griesinger, C.; Schwalbe, H.; Bax, A.; Torchia, D. A. *J. Magn. Reson.* **1992**, *100*, 538−558.

(21) Eriksson, A. E.; Baase, W. A.; Zhang, X. J.; Heinz, D. W.; Blaber, M.; Baldwin, E. P.; Matthews, B. W. *Science* **1992**, *255*, 178−183.

(22) Eriksson, A. E.; Baase, W. A.; Wozniak, J. A.; Matthews, B. W. *Nature* **1992**, *355*, 371−373.

(23) Eriksson, A. E.; Baase, W. A.; Matthews, B. W. *J. Mol. Biol.* **1993**, *229*, 747−769.

(24) Feher, V. A.; Baldwin, E. P.; Dahlquist, F. W. *Nat. Struct. Biol.* **1996**, *3*, 516−521.

(25) Matsumura, M.; Becktel, W. J.; Matthews, B. W. *Nature* **1988**, *334*, 406−410.

(26) Mulder, F. A. A.; Hon, B.; Muhandiram, D. R.; Dahlquist, F. W.; Kay, L. E. *Biochemistry* **2000**, *39*, 12614−12622.

(27) Yuan, T.; Vogel, H. J. *J. Biol. Chem.* **1998**, *273*, 30328−30335.

(28) Markley, J. L.; Jorsley, W. J.; Klein, M. P. *J. Chem. Phys.* **1971**, *55*, 3604−3607.

(29) Delaglio, F.; Grzesiek, S.; Vuister, G. W.; Zhu, G.; Pfeifer, J.; Bax, A. *J. Biomol. NMR* **1995**, *6*, 277−293.

(30) Luz, Z.; Meiboom, S. *J. Chem. Phys.* **1963**, *39*, 366−370.

(31) Carver, J. P.; Richards, R. E. *J. Magn. Reson.* **1972**, *6*, 89−105.

successively more complex models (i−iii), and only in cases where more complex models were justified were they used. Errors in parameters were estimated by a Monte Carlo fitting procedure[36] in which the errors for each dispersion profile have been obtained from the three repeat data sets (field strengths of 150, 500, and 1000 Hz, see above).

Deuterium spin relaxation experiments[11] were recorded on an ^{15}N/^{13}C, 50% ^{2}H-labeled sample of L99A to probe ps−ns time scale dynamics at methionine positions. Details of the experimental setup and data analysis are as described in Mulder et al.[26]

Simulations. Simulations of the evolution of the methyl spin system during the course of the experiment of Figure 1 were carried out using the spin operator basis $\vec{V}$ of eq 3 (see below). In the absence of chemical exchange and neglecting pulse imperfections and off-resonance effects, the evolution can be modeled using the relaxation matrices, $\tilde{\Gamma}_{I} + \tilde{\Gamma}_{E}$, the scalar coupling matrix $\pm i\tilde{J}$, and matrices describing the effects of the assumed perfect pulses (see eq 4 below and Appendix I). The elements of the relaxation matrices have been calculated in analytical form using a program written with Maple symbolic computation software (Waterloo Inc.). All dipolar interactions within the methyl group as well as the assumed axially symmetric CSA interaction for the ^{13}C spin[8] have been taken into account. The resulting auto- and cross-correlated relaxation terms with multiple spectral densities were included in full in the expressions for $\tilde{\Gamma}_{I}$. The spectral densities for intra-methyl interactions were calculated using the model-free formalism according to:[37−40]

$$J_{a,b}(\omega) = S_{\text{axis}}^{2}S_{\text{axis},a}S_{\text{axis},b}\frac{1}{5}\frac{\tau_{\text{r}}}{1 + \omega^{2}\tau_{\text{r}}^{2}} +$$
$$\{P_{2}(\cos\theta_{a,b}) - S_{\text{axis}}^{2}S_{\text{axis},a}S_{\text{axis},b}\}\frac{1}{5}\frac{\tau_{\text{c}}}{1 + \omega^{2}\tau_{\text{c}}^{2}} \quad (1)$$

In eq 1 a and b are vectors representing the pair of axially symmetric interactions that make an angle $\theta_{a,b}$ with each other, $(1/\tau_{\text{c}}) = (1/\tau_{\text{r}}) + (1/\tau_{\text{e}})$ with τ_{r} and τ_{e} the correlation times of overall tumbling and fast local motion respectively, S_{axis} is the order parameter for the bond between the methyl carbon and the directly attached heavy atom (i.e., three-fold symmetry axis of the methyl group) which reflects fast side-chain dynamics, and $S_{\text{axis},a}$, $S_{\text{axis},b}$ are the order parameters due to fast rotation of the methyl group about its three-fold axis, $S_{\text{axis},x} = P_{2}(\cos\theta_{\text{axis},x})$.

In addition, we have considered contributions from dipolar interactions between the spins of the methyl group and external protons, $\tilde{\Gamma}_{E}$, including all auto- and cross-correlated interactions but without extending the basis $\vec{V}$.[41,42] Spectral density functions of the same form as in eq 1 were used for dipolar interactions involving external protons, c, and evaluated assuming that the methyl group is static. Note that $S_{\text{axis},c}$ is set equal to 1.0 in this case and is no longer defined as above. The differences between static and dynamic pictures of methyl groups are likely to be small insofar as relaxation from external protons is concerned because of the approximate "spherically symmetric" distribution of the external protons in the vicinity of the methyl group. A more rigorous analysis of this approximation is beyond the scope of the present work.

The analytical expressions for the elements of the 6 × 6 relaxation matrix $\tilde{\Gamma}_{I} + \tilde{\Gamma}_{E}$ (see below) were further evaluated on the basis of the motional and structural parameters of T4 lysozyme. The calculations were performed for five methionine residues found in this protein using the set of atomic coordinates 6LZM[21] (the structure was protonated and refined using the program CNS[43]). Relaxation contributions from all external protons within a 6 Å radius of each methionine ^{13}C$^{\epsilon}$ were taken into account. Order parameters, S_{axis}^{2}, in the range from 0.30 to 0.98 were obtained from ^{2}H relaxation measurements on L99A.[26] Standard methyl group geometry was used to obtain the values of the order parameter $S_{\text{axis},x}$ for interactions within the methyl group. Finally, an overall tumbling time $\tau_{\text{r}} = 10.8$ ns was employed,[26] and the local correlation time was set to the average value observed in ^{2}H relaxation studies,[44] $\tau_{\text{e}} = 40$ ps, or alternatively, to zero, $\tau_{\text{e}} = 0$. Dispersion profiles were calculated for each of the five methionine residues. Results are illustrated for a single residue, Met 106, which represents one of the less favorable cases ($S_{\text{axis}}^{2} = 0.40$, see discussion below).

Results and Discussion

Theoretical Considerations. Figure 1 illustrates the pulse scheme used to quantitate slow exchange processes involving ^{13}C-labeled methyl groups in proteins. The experiment is essentially a ^{1}H−^{13}C HSQC modified to include a pair of variable pulse spacing, constant-time CPMG elements,[45,46] composed of the building blocks $(\tau - 180°_{y} - \tau)_{n/2}$ and $(\tau - 180°_{x} - \tau)_{n/2}$ denoted by CPMG$_{Y}$ and CPMG$_{X}$, respectively, in Figure 1. A series of 2D data sets are recorded by varying the number of 180° pulses and hence τ, with T kept constant. Intensities of cross-peaks are obtained from spectra recorded in this manner as a function of effective rf field strength, $\nu_{\text{CPMG}} = 1/(4\tau_{\text{CPMG}})$, with $2\tau_{\text{CPMG}} = 2\tau + pw_{\text{C}}^{180°}$, where 2τ is the time between successive pulses and $pw_{\text{C}}^{180°}$ is the length of each ^{13}C refocusing pulse. As described previously,[19] intensities of cross-peaks obtained for each ν_{CPMG} value are converted into effective decay rates, R_{2}^{eff}, according to the relation

$$R_{2}^{\text{eff}}(\nu_{\text{CPMG}}) = \frac{-1}{T}\ln\left(\frac{I(\nu_{\text{CPMG}})}{I_{\text{o}}}\right) \quad (2)$$

where $I(\nu_{\text{CPMG}})$ and I_{o} are intensities for a given cross-peak from spectra recorded with or without the two CPMG intervals (periods $a−b$ and $c−d$).

The ^{13}C relaxation properties of methyl groups are complicated by significant cross-correlation effects involving pairs of dipole interactions within the methyl spin system.[20,39,47] Magnetization modes can relax, therefore, with very different rates. Additionally, scalar coupling interconverts these modes so that it might be expected that relaxation dispersion profiles would depend critically on the number of ^{13}C refocusing pulses and hence on ν_{CPMG} even in the absence of exchange. In principle, the application of high-power ^{1}H decoupling during each CPMG element in Figure 1 would suppress evolution due to scalar coupling. However, care must be taken to ensure that the decoupling performance does not change as a function of ν_{CPMG}. In addition, decoupling does not completely simplify the

(32) Davies, D. G.; Perlman, M. E.; London, R. E. *J. Magn. Reson., Ser. B* **1994**, *104*, 266−275.

(33) Bloom, M.; Reeves, L. W.; Wells, E. J. *J. Chem. Phys.* **1965**, *42*, 1615−1624.

(34) Millet, O.; Loria, J. P.; Kroenke, C. D.; Pons, M.; Palmer, A. G. *J. Am. Chem. Soc.* **2000**, *122*, 2867−2877.

(35) Mosteller, F.; Tukey, J. W. *Data Analysis and Regression: A Second Course in Statistics*; Addison-Wesley: Reading, MA, 1977.

(36) Kamith, U.; Shriver, J. W. *J. Biol. Chem.* **1989**, *264*, 5586−5592.

(37) Lipari, G.; Szabo, A. J. *Am. Chem. Soc.* **1982**, *104*, 4559−4570.

(38) Lipari, G.; Szabo, A. *J. Am. Chem. Soc.* **1982**, *104*, 4546−4559.

(39) Kay, L. E.; Torchia, D. A. *J. Magn. Reson.* **1991**, *95*, 536−547.

(40) Daragan, V. A.; Mayo, K. H. *J. Magn. Reson., Ser. B* **1995**, *107*, 274−278.

(41) Khazanovich, T. N.; Zitserman, V. Y. *Mol. Phys.* **1971**, *21*, 65−82.

(42) Skrynnikov, N. R.; Khazanovich, T. N.; Sanctuary, B. C. *Mol. Phys.* **1997**, *91*, 977−992.

(43) Brünger, A. T.; Adams, P. D.; Clore, G. M.; DeLano, W. L.; Gros, P.; Grosse-Kunstleve, R. W.; Jiang, J.; Kuszewski, J.; Nilges, M.; Pannu, N. S.; Read, R. J.; Rice, L. M.; Simonson, T.; Warren, G. L. *Acta Crystallogr.* **1998**, *D54*, 905−921.

(44) Kay, L. E.; Muhandiram, D. R.; Farrow, N. A.; Aubin, Y.; Forman-Kay, J. D. *Biochemistry* **1996**, *35*, 361−368.

(45) Carr, H. Y.; Purcell, E. M. *Phys. Rev.* **1954**, *4*, 630−638.

(46) Meiboom, S.; Gill, D. *Rev. Sci. Instrum.* **1958**, *29*, 688−697.

(47) Palmer, A. G.; Wright, P. E.; Rance, M. *Chem. Phys. Lett.* **1991**, *185*, 41−46.

$$
\vec{V} = \begin{vmatrix}
C_+ \\[4pt]
\dfrac{2}{\sqrt{3}}C_+(H_{Z,1} + H_{Z,2} + H_{Z,3}) \\[6pt]
\dfrac{4}{\sqrt{3}}C_+(H_{Z,1}H_{Z,2} + H_{Z1}H_{Z,3} + H_{Z,2}H_{Z,3}) \\[6pt]
8C_+H_{Z,1}H_{Z,2}H_{Z,3} \\[4pt]
\dfrac{2}{\sqrt{6}}C_+(H_{+,1}H_{-,2} + H_{-,1}H_{+,2} + H_{+,1}H_{-,3} + H_{-,1}H_{+,3} + H_{+,2}H_{-,3} + H_{-,2}H_{+,3}) \\[6pt]
\dfrac{4}{\sqrt{6}}C_+(H_{+,1}H_{-,2}H_{Z,3} + H_{-,1}H_{+,2}H_{Z,3} + H_{+,1}H_{Z,2}H_{-,3} + H_{-,1}H_{Z,2}H_{+,3} + H_{Z,1}H_{+,2}H_{-,3} + H_{Z,1}H_{-,2}H_{+,3})
\end{vmatrix} \tag{3}
$$

relaxation, since a number of contributions, such as $^1\text{H}-^{13}\text{C}$ dipole−dipole cross-correlation (see below), are not suppressed. We therefore prefer the scheme illustrated in Figure 1, and in the discussion that follows we show that for the case of an isolated methyl group attached to a molecule tumbling slowly, *flat dispersion profiles are obtained in the absence of exchange using this sequence*. Subsequently, we demonstrate that relaxation from external protons does not change the flat character of dispersion profiles so long as the pulse scheme of Figure 1 is employed. In this regard the element extending from points *b* to *c* in Figure 1 (referred to in what follows as a P-element) which interconverts magnetization modes in a way so as to effectively equalize contributions from external protons to the relaxation of each mode is absolutely critical (see below). It is noteworthy that the P-element building block was originally conceived by Palmer and co-workers[17] for the case of averaging contributions from external proton spins in CPMG experiments recorded on AX spin systems and subsequently shown by Mulder et al. to be critical for applications involving AX$_2$ systems as well.[19] Thus, use of the P-element for averaging effects of external protons in CPMG experiments appears quite general. Next it is shown *that exchange parameters can be extracted from dispersion curves using simple equations derived for an isolated spin exchanging between two sites* so long as the relaxation properties of the methyl group in each exchanging site are identical. Finally, numerical simulations are provided which further establish the validity of the methodology.

The Dispersion Profile of Isolated Methyl Groups in the Absence of Exchange Is Flat. At point *a* in the pulse scheme of Figure 1 the magnetization of interest is given by C_Y, which subsequently evolves during the course of the sequence under the influence of pulses, scalar couplings, and spin relaxation. In what follows this evolution is described in terms of the time dependence of the vector $\vec{V}$ comprised of the six symmetrized magnetization modes[48] needed to describe transverse relaxation in an isolated methyl group,[49] eq 3, where $C_+ = C_X + iC_Y$ and each of the methyl protons are identified by the subscripts 1−3. Below, the second, third, fifth, and sixth elements of the basis $\vec{V}$ (eq 3) will be denoted by $2/\sqrt{3}C_+H_Z$, $4/\sqrt{3}C_+H_ZH_Z$, $2/\sqrt{6}C_+H_+H_-$ and $4/\sqrt{6}C_+H_+H_-H_Z$ respectively. Evolution of magnetization during a given τ interval of the CPMG$_Y$ scheme can be calculated according to

$$
\frac{\mathrm{d}}{\mathrm{d}t}\vec{V} = -(i\tilde{Z} + i\tilde{J} + \tilde{\Gamma}_\mathrm{l})\vec{V} \tag{4.1}
$$

(48) Corio, P. L. *Structure of High-Resolution NMR Spectra*; Academic Press: New York, 1966.
(49) Kay, L. E.; Bull, T. E. *J. Magn. Reson.* **1992**, *99*, 615−622.

or

$$
\frac{\mathrm{d}}{\mathrm{d}t}\vec{V} = -(-i\tilde{Z} - i\tilde{J} + \tilde{\Gamma}_\mathrm{l})\vec{V} \tag{4.2}
$$

depending on whether an even (eq 4.1) or odd (eq 4.2) number of ^{13}C refocusing pulses have been applied prior to the τ interval. In eq 4 $\tilde{Z}$, $\tilde{J}$ and $\tilde{\Gamma}_\mathrm{l}$ are matrices which include the effects of chemical shift ($\tilde{Z}$) and scalar coupling ($\tilde{J}$) evolution as well as relaxation from spins internal to the methyl spin system ($\tilde{\Gamma}_\mathrm{l}$). Differences between eqs 4.1 and 4.2 result from the fact that ^{13}C 180° pulses invert the sense of precession due to chemical shift or scalar coupling (i.e., interconvert C_+ and C_-) but do not affect evolution due to relaxation. In the description that follows only the zero-frequency spectral density terms are included in the relaxation matrix (macromolecular limit). Later, in the course of numerical simulations all of the spectral density terms will be considered. The elements of the 6×6 matrices, $\tilde{Z}$, $\tilde{J}$, and $\tilde{\Gamma}_\mathrm{l}$, evaluated in the basis of eq 3 are given in Appendix I.

Starting from eq 4 it is straightforward to show that between points *a* and *d*, corresponding to the scheme $\{\tau - 180°_y - 2\tau - 180°_y - \tau\}_{n/4} P\{\tau - 180°_x - 2\tau - 180°_x - \tau\}_{n/4}$, evolution of magnetization proceeds according to

$$
\vec{V}(T) = \prod_{k=1}^{n/4}\{e^{-(-i\tilde{Z}-i\tilde{J}+\tilde{\Gamma}_\mathrm{l})\tau}\,e^{-(i\tilde{Z}+i\tilde{J}+\tilde{\Gamma}_\mathrm{l})2\tau}\,e^{-(-i\tilde{Z}-i\tilde{J}+\tilde{\Gamma}_\mathrm{l})\tau}\} \times
$$
$$
\tilde{P}\prod_{k=1}^{n/4}\{e^{-(i\tilde{Z}+i\tilde{J}+\tilde{\Gamma}_\mathrm{l})\tau}\,e^{-(-i\tilde{Z}-i\tilde{J}+\tilde{\Gamma}_\mathrm{l})2\tau}\,e^{-(i\tilde{Z}+i\tilde{J}+\tilde{\Gamma}_\mathrm{l})\tau}\}\vec{V}(0) \tag{5}
$$

where $\vec{V}(0)$ is the initial magnetization state at point *a* and $\tilde{P}$ is a matrix which describes evolution between points *b* and *c* in the scheme of Figure 1 (P-element), with $\zeta = 1/(4J_\mathrm{CH})$. Neglecting for the moment relaxation during ζ,

$$
\tilde{P} = i\begin{vmatrix}
0 & 0 & 0 & 1 & 0 & 0 \\
0 & 0 & -1 & 0 & 0 & 0 \\
0 & 1 & 0 & 0 & 0 & 0 \\
-1 & 0 & 0 & 0 & 0 & 0 \\
0 & 0 & 0 & 0 & 0 & -1 \\
0 & 0 & 0 & 0 & 1 & 0
\end{vmatrix} \tag{6}
$$

Although the P-element is of little importance in the case of an isolated spin system, we show below that it is critical when external protons are considered. Equation 5 can be simplified considerably by noting that $\tilde{Z}$, $\tilde{J}$, and $\tilde{\Gamma}_\mathrm{l}$ commute with each other (see matrices in Appendix I) arriving at,

$$
\vec{V}(T) = e^{-(\tilde{\Gamma}_\mathrm{l}+\tilde{P}\tilde{\Gamma}_\mathrm{l}\tilde{P}^{-1})T}\tilde{P}\vec{V}(0) \tag{7}
$$

where $\tilde{P}^{-1} = \tilde{P}$ and we have made use of the relation $\tilde{P}\tilde{J}\tilde{P}^{-1} = -\tilde{J}$, which can be verified directly from the matrix definitions in Appendix I and eq 6. The evolution of magnetization modes $\vec{V}$ over the constant-time relaxation period T is thus independent of the number of 180° pulses, n, as can be seen from eq 7. As a result, completely flat dispersion profiles are obtained so that R_2^{eff} values are constant and depend only on the relaxation properties of the spin system, $\tilde{\Gamma}_I + \tilde{P}\tilde{\Gamma}_I\tilde{P}^{-1}$.

It is noteworthy that $\tilde{\Gamma}_I$ and $\tilde{P}\tilde{\Gamma}_I\tilde{P}^{-1}$ differ only in that the signs of the elements resulting from cross-correlation between $^{13}C-^1H$ dipolar and ^{13}C chemical shift anisotropy relaxation interactions are inverted (see matrices in Appendix I). Thus, the effect of the P-element is to refocus these cross-correlation interactions.

The commutativity between $\tilde{\Gamma}_I$ and the scalar coupling and chemical shift matrices is quite remarkable and, as shown in Appendix II, derives from the fact that the superoperators describing evolution due to relaxation, chemical shift, and scalar coupling commute. This holds only in the macromolecular limit where the relaxation is dominated by spectral density elements evaluated at zero frequency.

Influence of External Protons on Relaxation Dispersion Profiles. As described above the fact that $[\tilde{J},\tilde{\Gamma}_I] = 0$ ensures that flat dispersion profiles are obtained for isolated methyl groups in the absence of chemical exchange. However, the high density of methyl groups in hydrophobic cores of proteins[50] leads to a large number of interactions with external proton spins, and any experimental scheme must take into account relaxation contributions from these neighbors. In the presence of external proton spins, evolution of $\vec{V}$ between ^{13}C refocusing pulses during the CPMG pulse trains is given by

$$\frac{d}{dt}\vec{V} = -(\pm i\tilde{Z} \pm i\tilde{J} + \tilde{\Gamma}_I + \tilde{\Gamma}_E)\vec{V} \quad (8)$$

where the matrix $\tilde{\Gamma}_E$ includes contributions from all external spins (in the present consideration $\tilde{\Gamma}_E$ is confined to the basis of the six magnetization modes $\vec{V}$[41,42]). In Appendix I the $\tilde{\Gamma}_E$ matrix is presented for the case of external relaxation from a single proton spin attached to a macromolecule in the slow tumbling regime. It can be immediately verified that $[\tilde{J},\tilde{\Gamma}_E] \neq 0$ (see also Appendix II) so that relaxation dispersion profiles generated from simple CPMG schemes (i.e., without the P-element in Figure 1) show pronounced dependence on ν_{CPMG} even in the absence of chemical exchange (see below). On a qualitative level, the effect of external protons is to increase the effective relaxation rates of individual magnetization modes by different amounts, and it is this differential relaxation that causes the problem. Specifically, in the macromolecular limit, external protons increase the relaxation rates of the first four elements of $\vec{V}$, C_+, $2/\sqrt{3}C_+H_Z$, $4/\sqrt{3}C_+H_ZH_Z$, and $8C_+H_{Z,1}H_{Z,2}H_{Z,3}$, by 0, $(1/T_{1,S})$, $(2/T_{1,S})$, and $(3/T_{1,S})$, respectively, where $(1/T_{1,S})$ is the methyl proton–external proton spin flip rate (see Appendix I). The P-element in the center of the sequence interconverts modes 1 and 4 as well as 2 and 3 (and 5 and 6) so that the effective relaxation rate of each of the four modes is elevated by the uniform amount of $(3/2)(1/T_{1,S})$. If the relaxation of each element of $\vec{V}$ is increased uniformly, then $\tilde{\Gamma}_E$ is effectively diagonal, $[\tilde{J},\tilde{\Gamma}_E] = 0$, and J-coupled evolution can be fully refocused.

A more rigorous description of the utility of the P-element in Figure 1 can be given by considering evolution of magnetiza-

tion between points a and d in the simple case where $(n/4) = 1$. Following eq 5 we can write,

$$\vec{V}(T) = \{e^{-\tilde{A}\tau} e^{-\tilde{B}\tau} e^{-\tilde{B}\tau} e^{-\tilde{A}\tau}\}\tilde{P}\{e^{-\tilde{B}\tau} e^{-\tilde{A}\tau} e^{-\tilde{A}\tau} e^{-\tilde{B}\tau}\}\vec{V}(0) \quad (9)$$

where $\tilde{A} = -i\tilde{Z} - i\tilde{J} + \tilde{\Gamma}_I + \tilde{\Gamma}_E$ and $\tilde{B} = i\tilde{Z} + i\tilde{J} + \tilde{\Gamma}_I + \tilde{\Gamma}_E$. Equation 9 can be simplified by the consecutive application of the Baker–Campbell–Hausdorff formula[51] to pairs of exponentials (starting from $e^{-\tilde{A}\tau}e^{-\tilde{B}\tau}$, $e^{-\tilde{B}\tau}e^{-\tilde{A}\tau}$), so that

$$\vec{V}(T) \approx e^{-\tilde{Q}}\tilde{P}\vec{V}(0) \quad (10)$$

where to third order,

$$\tilde{Q} = 4(\tilde{\Gamma}_T + \tilde{P}\tilde{\Gamma}_T\tilde{P}^{-1})\tau + 8[\tilde{\Gamma}_T,\tilde{P}\tilde{\Gamma}_T\tilde{P}^{-1}]\tau^2 + \frac{2}{3}[\tilde{J},[\tilde{J},\tilde{\Gamma}_T + \tilde{P}\tilde{\Gamma}_T\tilde{P}^{-1}]]\tau^3 + [[\tilde{J},\tilde{\Gamma}_T],\tilde{\Gamma}_T - \tilde{P}\tilde{\Gamma}_T\tilde{P}^{-1}]\tau^3 \quad (11)$$

with $\tilde{\Gamma}_T = \tilde{\Gamma}_I + \tilde{\Gamma}_E$. Note that to first and second order the matrix $\tilde{Q}$ is independent of $\tilde{J}$. The leading third-order term is proportional to $\tilde{J}^2$ and to $\tilde{\Gamma}_T + \tilde{P}\tilde{\Gamma}_T\tilde{P}^{-1}$. Assuming that the magnitude of the third term is on the order of an average element from the matrix product $\tilde{J}^2(\tilde{\Gamma}_T + \tilde{P}\tilde{\Gamma}_T\tilde{P}^{-1})\tau^3$, this term could contribute as much as 30% to the total of $\tilde{Q}$, for $\tau = 5$ ms. In fact, however, the design of the P-element is such that this term is 0. Noting that $[\tilde{J},\tilde{\Gamma}_I] = 0$ it follows that

$$[\tilde{J},[\tilde{J},\tilde{\Gamma}_T + \tilde{P}\tilde{\Gamma}_T\tilde{P}^{-1}]] = [\tilde{J},[\tilde{J},\tilde{\Gamma}_E + \tilde{P}\tilde{\Gamma}_E\tilde{P}^{-1}]] \quad (12)$$

and from the matrix definitions in Appendix I, it can be shown that

$$[\tilde{J},\tilde{\Gamma}_E + \tilde{P}\tilde{\Gamma}_E\tilde{P}^{-1}] = 0 \quad (13)$$

The final term in eq 11 depends on J to first order and contributes less than several percent to $\tilde{Q}$. Thus, interconversion of magnetization modes via use of the P-element in the sequence of Figure 1 allows the system to evolve in a manner that is essentially independent of scalar coupling and is a function of spin relaxation alone. Since the relaxation of the methyl spin system is independent of the number of ^{13}C pulses in the CPMG trains, it follows that the evolution of $\vec{V}$ does not depend on ν_{CPMG} in the absence of chemical exchange.

In principle, the P-element is expected to be most effective when $T < T_{1,S}$. In practice this condition is almost always fulfilled since the delay T in the sequence of Figure 1 is set to a value less than the effective relaxation time and consequently less than $T_{1,S}$. Numerical simulations have established that the P-element performs well even outside this limit. For example, computations performed for $\tau_r = 10.8$ ns, $T = 200$ ms and $\tau_r = 20$ ns, $T = 40$ ms using the basis set indicated in eq 3 show that in the absence of exchange the dispersion profiles are flat, with variation of R_2^{eff} less than 1 s^{-1}.

Chemical Exchange Can Be Analyzed in a Straightforward Manner. The theory described above demonstrates that in the macromolecular limit, and in the absence of exchange, flat dispersion profiles are obtained for a methyl group if the pulse scheme of Figure 1 is employed. In what follows below, we consider the case of chemical exchange between two sites with the same relaxation properties and show that accurate exchange parameters can be extracted from fits of dispersion curves using equations derived for an isolated single spin

(50) Janin, J.; Miller, S.; Chothia, C. *J. Mol. Biol.* **1988**, *204*, 155–164.

(51) Ernst, R. R.; Bodenhausen, G.; Wokaun, A. *Principles of Nuclear Magnetic Resonance in One and Two Dimensions*; Oxford University Press: Oxford, 1987.

undergoing two-site exchange.[31,32] During each τ period between ^{13}C refocusing pulses in the CPMG trains of Figure 1 the evolution of $\vec{V}$ is given by

$$\frac{d}{dt}\begin{pmatrix}\vec{V}_a \\ \vec{V}_b\end{pmatrix} =$$

$$-\begin{pmatrix}\pm i\tilde{J} + \tilde{\Gamma}_T + \tilde{K}_{a\to b} \pm i\tilde{Z}_a & -\tilde{K}_{b\to a} \\ -\tilde{K}_{a\to b} & \pm i\tilde{J} + \tilde{\Gamma}_T + \tilde{K}_{b\to a} \pm i\tilde{Z}_b\end{pmatrix}\begin{pmatrix}\vec{V}_a \\ \vec{V}_b\end{pmatrix} \tag{14}$$

where the basis has been extended to include the six magnetization modes pertaining to site a, $\vec{V}_a$, and their counterparts for site b, $\vec{V}_b$, with the modes weighted by the populations p_a and p_b, respectively. Equation 14 is given in symbolic form, with $\tilde{J}$, $\tilde{\Gamma}_T$, $\tilde{Z}_a$ and $\tilde{Z}_b$ denoting 6×6 matrices as described above (see Appendix I), $\tilde{K}_{a\to b} = k_{a\to b}\tilde{E}$, $\tilde{K}_{b\to a} = k_{b\to a}\tilde{E}$, where $\tilde{E}$ is the 6×6 identity matrix and $k_{a\to b}$, $k_{b\to a}$ are the rate constants for the exchange between sites a and b. Noting that

$$\left[\begin{pmatrix}\pm i\tilde{J} + \tilde{\Gamma}_T & 0\tilde{E} \\ 0\tilde{E} & \pm i\tilde{J} + \tilde{\Gamma}_T\end{pmatrix}, \begin{pmatrix}\tilde{K}_{a\to b} \pm i\tilde{Z}_a & -\tilde{K}_{b\to a} \\ -\tilde{K}_{a\to b} & \tilde{K}_{b\to a} \pm i\tilde{Z}_b\end{pmatrix}\right] = 0 \tag{15}$$

it follows that evolution due to scalar coupling and relaxation can be treated separately from evolution due to chemical shift and exchange. Additionally, the results of the last section establish that to a very good approximation scalar coupling effects are refocused by the sequence of Figure 1. It can be shown, therefore, that

$$\begin{pmatrix}\vec{V}_a(T) \\ \vec{V}_b(T)\end{pmatrix} \approx e^{-\tilde{R}T} \times$$

$$\prod_{k=1}^{n/4}\{e^{-\tilde{C}\tau} e^{-\tilde{D}2\tau} e^{-\tilde{C}\tau}\}\prod_{k=1}^{n/4}\{e^{-\tilde{D}\tau} e^{-\tilde{C}2\tau} e^{-\tilde{D}\tau}\}\tilde{P}\begin{pmatrix}\vec{V}_a(0) \\ \vec{V}_b(0)\end{pmatrix} \tag{16}$$

where

$$\tilde{C} = \begin{pmatrix}\tilde{K}_{a\to b} - i\tilde{Z}_a & -\tilde{K}_{b\to a} \\ -\tilde{K}_{a\to b} & \tilde{K}_{b\to a} - i\tilde{Z}_b\end{pmatrix} \tag{17.1}$$

$$\tilde{D} = \begin{pmatrix}\tilde{K}_{a\to b} + i\tilde{Z}_a & -\tilde{K}_{b\to a} \\ -\tilde{K}_{a\to b} & \tilde{K}_{b\to a} + i\tilde{Z}_b\end{pmatrix} \tag{17.2}$$

and from eq 11

$$\tilde{R} =$$

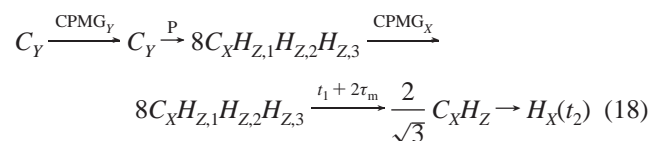$$\frac{1}{2}\begin{pmatrix}\tilde{\Gamma}_T + \tilde{P}\tilde{\Gamma}_T\tilde{P}^{-1} + \frac{1}{4}[\tilde{\Gamma}_T, \tilde{P}\tilde{\Gamma}_T\tilde{P}^{-1}]T & 0\tilde{E} \\ 0\tilde{E} & \tilde{\Gamma}_T + \tilde{P}\tilde{\Gamma}_T\tilde{P}^{-1} + \frac{1}{4}[\tilde{\Gamma}_T, \tilde{P}\tilde{\Gamma}_T\tilde{P}^{-1}]T\end{pmatrix} \tag{17.3}$$
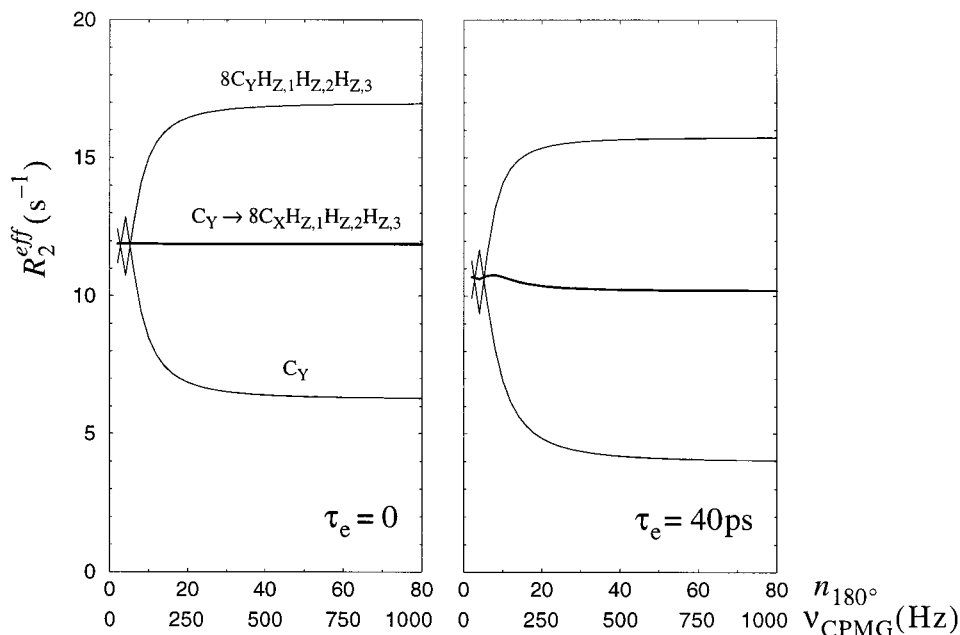
In eq 16 the term $\exp(-\tilde{R}T)$ is a matrix that does not depend on the number of 180° pulses, n. The remaining part of the evolution operator originating from matrices $\tilde{C}$ and $\tilde{D}$ is comprised of 2×2 blocks which couple magnetization modes $\vec{V}_a$ and $\vec{V}_b$ (via exchange). The resulting relaxation dispersion curve is therefore equivalent to the one derived for a single isolated spin exchanging between two sites under the effect of the CPMG sequence. Thus, simple two site equations that have been described in the literature[31,32] can be used to interpret the dispersion profiles obtained with the pulse scheme of Figure 1.

Equation 16 indicates that, in principle, it is possible to measure the decay of the magnetization in a nonconstant time manner as a function of T, with the subsequent separation of relaxation and exchange contributions, in much the same way as is frequently done in the analysis of chemical exchange using AX spin systems. However, the decay of signal as a function of T is multiexponential (six exponents, see eq 16 and Appendix I) which precludes the accurate extraction of the relaxation rates. We therefore prefer the simpler approach of fixing T for all ν_{CPMG} values, recognizing, of course, that R_2^{eff} depends on the choice of T.
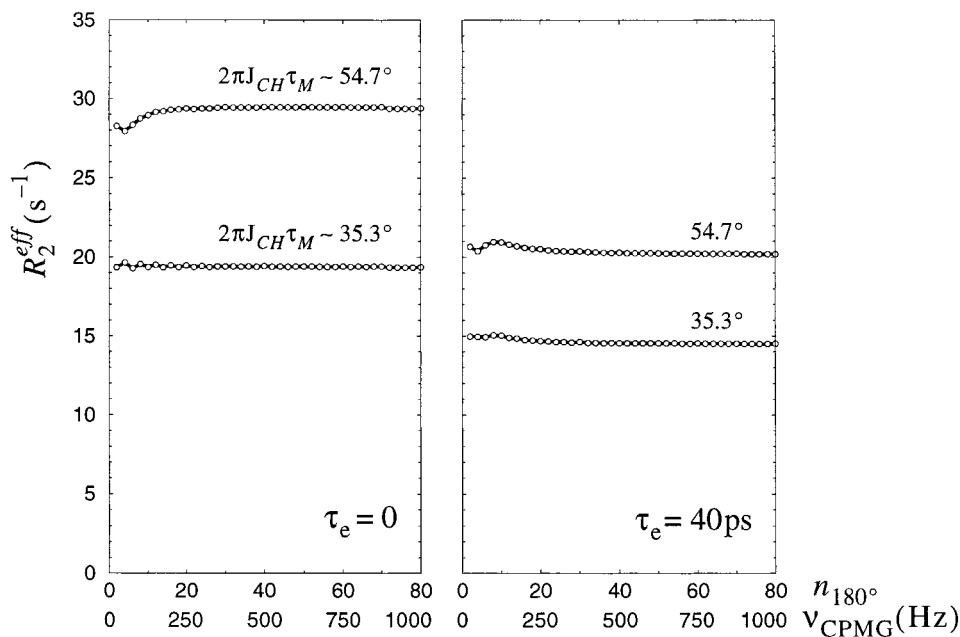
Numerical Simulations Validate the Methodology. The above discussion has focused on a methyl group attached to a macromolecule tumbling sufficiently slowly so that only the spectral density terms evaluated at zero frequency contribute to relaxation (the relaxation matrices in Appendix I are valid in this limit). In a series of simulations we have included (i) all of the spectral density terms that appear in the expressions for the complete relaxation matrix, (ii) relaxation contributions from external protons (see Materials and Methods), and (iii) the effects of relaxation and scalar coupling during the complete pulse scheme, including the P-element, the τ_M delays and the t_1 evolution time. Figure 2 illustrates the evolution of the operators C_Y and $8C_YH_{Z,1}H_{Z,2}H_{Z,3}$ during the interval extending from a to d in the scheme of Figure 1 with the P-element removed (thin lines in the plot). The simulated curves shown in Figure 2 are for methionine 106 in L99A with $S_{axis}^2 = 0.4$, $\tau_e = 0$, 40 ps and $\tau_r = 10.8$ ns. The relaxation dispersion profiles generated from the starting conditions, C_Y and $8C_YH_{Z,1}H_{Z,2}H_{Z,3}$, show considerable variation as a function of effective field, ν_{CPMG}, due to relaxation contributions from external proton spins, as expected from the results of the previous sections. However, insertion of the P-element ensures that dispersion profiles are essentially independent of ν_{CPMG}, in the absence of exchange (bold curves in Figure 2), as described in the previous sections. Notably, the dependence on ν_{CPMG} is slightly more pronounced for more slowly spinning methyl groups (compare bold faced profiles from $\tau_e = 0$ ps and $\tau_e = 40$ ps) since the spectral density terms evaluated at nonzero frequencies, $J(\omega)$, become larger as a function of increasing τ_e. Similarly, the dependence on ν_{CPMG} becomes more pronounced with decreasing S_{axis}^2, since the importance of the $J(0)$ terms relative to the higher frequency spectral densities, $J(\omega)$, is diminished. Recall that the analysis presented in a previous section which predicts completely flat dispersion curves is only valid in the macromolecular limit where relaxation is dominated by $J(0)$ components.

Figure 3 shows results obtained from simulations which include the evolution of magnetization during the complete pulse sequence of Figure 1 (from a to e). Simulated 2D data sets were generated for different values of ν_{CPMG} using the same dwell time and number of increments in the t_1 dimension as those employed in experimental measurements. These data sets are subsequently processed in a manner analogous to that for the experimental data. It is thus possible to evaluate the effect of cross-correlated relaxation during the interval extending from d to e in the pulse sequence as well. The basic net flow of magnetization during the sequence of Figure 1, neglecting cross-correlations for the moment, is

$$C_Y \xrightarrow{\text{CPMG}_Y} C_Y \xrightarrow{\text{P}} 8C_XH_{Z,1}H_{Z,2}H_{Z,3} \xrightarrow{\text{CPMG}_X}$$

$$8C_XH_{Z,1}H_{Z,2}H_{Z,3} \xrightarrow{t_1 + 2\tau_m} \frac{2}{\sqrt{3}}C_XH_Z \to H_X(t_2) \tag{18}$$

Figure 2. Relaxation dispersion profiles simulated with a number of different constant-time CPMG schemes in the absence of chemical exchange. The middle profile (bold line) corresponds to the scheme of Figure 1 with the P-element modeled by matrix $\tilde{P}$ of eq 6. The upper and lower profiles (thin lines) are obtained by eliminating the P-element in the sequence of Figure 1. The magnetization modes representing the initial spin states are indicated next to each curve. In the case of the middle profile, magnetization begins as C_Y and is converted to $8C_XH_{Z,1}H_{Z,2}H_{Z,3}$ by the P-element (hence the designation $C_Y \rightarrow 8C_XH_{Z,1}H_{Z,2}H_{Z,3}$). The simulations were carried out for the Met 106 methyl group of L99A, assuming a proton frequency of 600 MHz and a duration of the constant-time period $T = 40$ ms. The results are shown for two values of the local correlation time, $\tau_e = 0$ (left panel) and $\tau_e = 40$ ps (right panel). Details of the simulation protocols are provided in Materials and Methods.
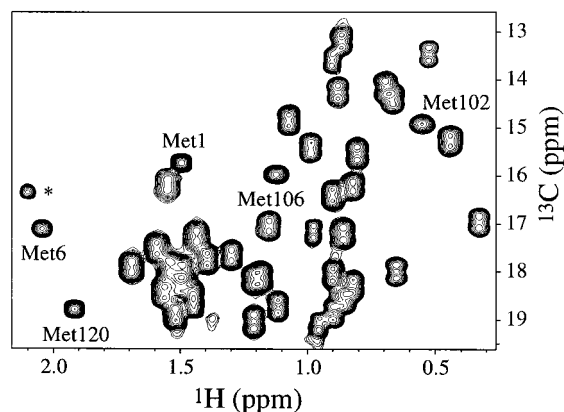

Figure 3. Relaxation dispersion profiles simulated for the CT-CPMG scheme of Figure 1 in the absence of chemical exchange. The simulation encompasses the period from a to e in the pulse sequence and makes use of parameters identical to those employed in the experimental setup (see Materials and Methods for details). The value of the delay τ_M is selected either with the aim of maximizing the transfer of the coherence $8C_+H_{Z,1}H_{Z,2}H_{Z,3}$ (point d in the sequence) into the coherence $2/\sqrt{3} \, C_+H_Z$ (point e) using $2\pi J_{CH}\tau_M = 54.7°$ or, alternatively, minimizing the transfer of $2/\sqrt{3} \, C_+H_Z$ from point d to point e ($2\pi J_{CH}\tau_M = 35.3°$). The corresponding values of τ_M that have been employed in the simulations are indicated in the plot next to the curves. Other conditions are the same as described in the legend of Figure 2. It is clear that flatter profiles are obtained with $2\pi J_{CH}\tau_M = 35.3°$, and we have therefore set τ_M accordingly in all experiments.

Maximal transfer of magnetization to protons for observation (during the period extending from d to e, denoted by $t_1 + 2\tau_m$ in eq 18) occurs for $2\pi J_{CH}\tau_M = 54.7°$. A more detailed analysis shows that in addition to the term of interest, $8C_XH_{Z,1}H_{Z,2}H_{Z,3}$, at point d in the sequence, a significant amount of magnetization of the form $2/\sqrt{3}C_XH_Z$ is present as well, originating from

^{13}C$-^1$H dipole$-$dipole cross-correlation interactions. Noting that the transfer of magnetization from this term to observable signal is proportional to $\cos^3(2\pi J_{CH}\tau_M) - 2 \, \sin^2(2\pi J_{CH}\tau_M) \cos(2\pi J_{CH}\tau_M)$, it is possible to set $2\pi J_{CH}\tau_M = 35.3°$ and hence block this transfer. Figure 3 illustrates that flatter dispersion profiles are obtained with $2\pi J_{CH}\tau_M = 35.3°$ (maximum varia-
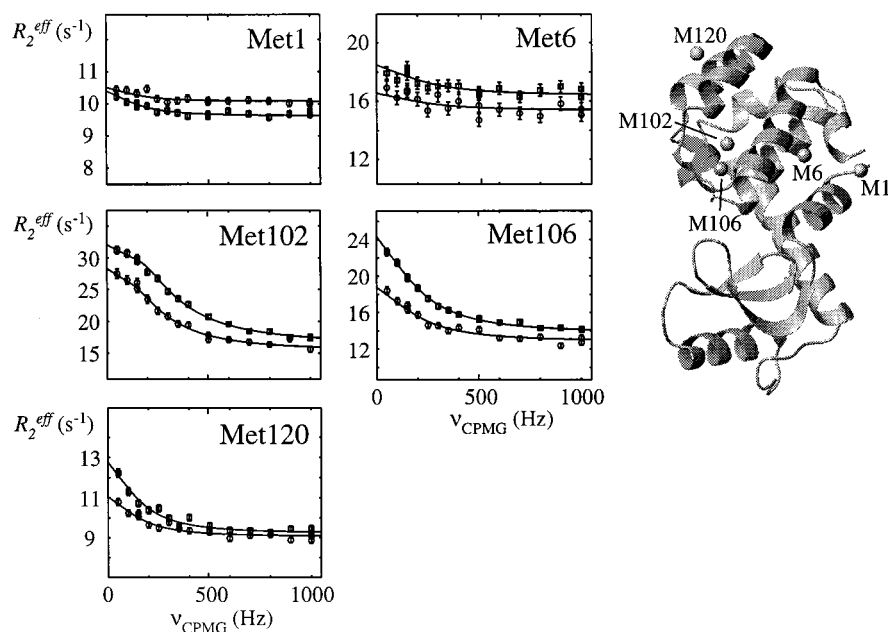
Figure 4. Two-dimensional $^1H-^{13}C$ correlation map of L99A recorded at 600 MHz using the scheme of Figure 1 with the CPMG periods eliminated (reference spectrum). Methionine cross-peaks are labeled. Cross-peaks arising from the (slight) degradation of the sample are indicated with a *.

tions of R_2^{eff} of 0.4 and 0.6 s^{-1} for $\tau_e = 0$, 40 ps, respectively, in the absence of exchange) then with $2\pi J_{CH}\tau_M = 54.7°$ (maximum variations of R_2^{eff} of 1.5 and 0.8 s^{-1} for $\tau_e = 0$, 40 ps) and we have therefore used the former setting in all of our experiments. To investigate the applicability of this method to smaller proteins simulations have also been repeated for $\tau_r = 5$ ns and maximal variations in R_2^{eff} of 0.04 and 0.6 s^{-1} for $\tau_e = 0$, 40 ps have been obtained with $2\pi J_{CH}\tau_M = 35.3°$. Finally, (near) flat dispersion profiles can also be obtained starting with magnetization of the form $2/\sqrt{3}C_YH_Z$ at point *a* in the sequence of Figure 1 and exchanging this coherence with $4/\sqrt{3}C_XH_ZH_Z$ via the P-element. However, the substantial (approximately 60%) increase in the relaxation rates of these terms relative to the C_Y, $8C_XH_{Z,1}H_{Z,2}H_{Z,3}$ pair (see Appendix I) indicates that starting from in-phase magnetization is preferable. Therefore, the experiment has been designed so that magnetization originates on carbon.

An Application to L99A. Figure 4 shows a 600 MHz 2D $^1H-^{13}C$ correlation map of a 1 mM uniformly $^{15}N/^{13}C$-labeled sample of L99A at 20 °C recorded with the sequence of Figure 1 with the periods from *a* to *b* and *c* to *d* removed (reference spectrum). All of the five methionine correlations are observed. Figure 5 illustrates relaxation dispersion profiles for each of the five methionine methyls obtained from spectra recorded at 600 (circles) and 800 (squares) MHz. *F*-statistic tests[35] show that dispersions for Met 1, 6, 106, and 120 are best fitted using the fast-exchange equation,[30] while Met 102 falls in the intermediate exchange regime with an estimated $\alpha = d \ln R_{ex}/d \ln B_o$ value of 0.7 and is therefore best fitted with the general two-site equation.[31,32] Reduced χ^2 values less than 1.5 are obtained for all fits, indicating that each of the dispersion profiles is well fit to the appropriate model. Exchange lifetimes, τ_{ex}, derived from this analysis vary from 0.66 to 0.96 ms (20 °C), with an average value of 0.84 ± 0.15 at 20 °C and 0.80 ± 0.30 at 25 °C. These values are in good agreement with average lifetimes obtained from relaxation dispersion profiles recorded for backbone amides, $\tau_{ex} = 0.86 ± 0.15$ ms measured for L99A at 25 °C.[26] The exchange parameters obtained from fits of the dispersion curves recorded at 20 °C are listed in Table 1. Because the motion of Met 102 is not in the fast-exchange regime, it is possible to extract the chemical shift difference, $|\omega_a - \omega_b|$, along with the relative populations of the two exchanging states, p_a and p_b, from fits of the relaxation dispersion profiles of this residue using the general equation for two-site exchange. In contrast, because the fast-exchange equation has been used to fit the profiles of the other methionines, only the product $p_ap_b(\omega_a - \omega_b)^2$ can be obtained. Assuming, however, that each of the methionine residues is reporting on the same processes it is possible to use the populations obtained from fits of the data for Met 102 to extract chemical shift differences between the exchanging states for all residues, as shown in Table 1. In this regard it is interesting to note that there is a reasonable correlation between proximity to the cavity and $|\omega_a - \omega_b|$, with the distance from the
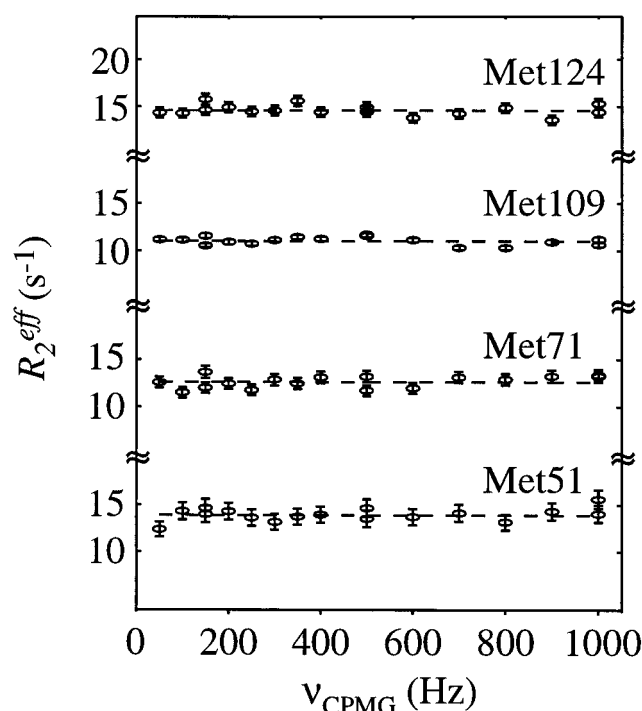

Figure 5. Relaxation dispersion profiles for the methionine residues in L99A. The solid lines correspond to the best fit curves generated from simultaneous fits of the data recorded at 600 (circles) and 800 (squares) MHz using the appropriate two-site exchange equation (see Table 1 and Materials and Methods). A ribbon diagram of the structure of L99A is displayed to the right of the dispersion curves, illustrating the positions of the methionines in the protein.

Table 1.   Relaxation Parameters for Methionine $^{13}C^{\epsilon}$ Spins in L99A at 20 °C

residue	fitting model[a]	τ_{ex}(ms)[b]	$p_a(\%)$[c]	$\omega_C^a - \omega_C^b$(ppm)[d]	R_2^{eff} ($\nu_{CPMG} \rightarrow \infty$)(s^{-1}) $\omega_0/2\pi$=600 MHz	$\omega_0/2\pi$=800 MHz	S_{axis}^2[e]
Met 1	FE	0.95 ± 0.20	−	0.16 ± 0.07	10.07 ± 0.03	9.62 ± 0.04	0.30 ± 0.01
Met 6	FE	0.66 ± 0.22	−	0.34 ± 0.19	15.35 ± 0.16	16.35 ± 0.21	0.98 ± 0.02
Met 102	GE	0.96 ± 0.13	2.1 ± 0.1	1.37 ± 0.05	15.28 ± 0.17	16.22 ± 0.25	0.67 ± 0.14
Met 106	FE	0.71 ± 0.05	−	0.69 ± 0.17	12.82 ± 0.12	13.70 ± 0.16	0.40 ± 0.02
Met 120	FE	0.92 ± 0.12	−	0.35 ± 0.11	9.05 ± 0.05	9.19 ± 0.08	0.31 ± 0.01

[a] Relaxation dispersion profiles, $R_2^{eff}(\nu_{CPMG})$, were fitted using the equation for the two-site fast-exchange (FE) process[30] and the general two-site equations valid for any exchange regime (GE).[31,32,34] The results of the two fitting procedures were compared using F-test statistics.[35] The GE model leads to a statistically significant improvement over the FE model only in the case of Met 102. [b] $\tau_{ex} = (k_{a \rightarrow b} + k_{b \rightarrow a})^{-1}$, where $k_{a \rightarrow b}$ and $k_{b \rightarrow a}$ are the rates of conversion between the two conformers. The uncertainty in τ_{ex} and other parameters have been estimated using a Monte Carlo analysis as described in the text. [c] Population of the minor conformer. [d] Chemical shift difference between the $^{13}C^{\epsilon}$ resonances in the two conformations. When using the FE model only the product $p_a(1 - p_a)(\omega_C^a - \omega_C^b)^2$ can be extracted from the analyses of the relaxation dispersion profiles. Assuming that $p_a = 2.1\%$ (Met 102) the magnitude of $\omega_C^a - \omega_C^b$ for other methionine residues is obtained from the above product. [e] Order parameter (squared) for the three-fold symmetry axis of the methyl group (i.e. the bond between methyl ^{13}C and the directly attached sulfur atom) as determined from ^2H relaxation measurements.

Figure 6.   Relaxation dispersion profiles (600 MHz) of selected methionine residues in a calmodulin−peptide complex. The results provide experimental proof that in the absence of exchange flat dispersion profiles are obtained using the pulse scheme of Figure 1.

methyl group to the cavity increasing in the following order, Met 102 < Met 106 < Met 6 < Met 120 < Met 1.

In addition to the slow dynamics measurements described above we have also probed ps−ns time scale methyl dynamics of the methionine residues via the measurement of ^2H spin relaxation properties of $^{13}CH_2D$ methyls.[11] Values of S_{axis}^2, describing the amplitude of $C^{\epsilon}-S$ bond vector motions are listed in the Table as well. S_{axis}^2 values vary from 0.98 (Met 6) to 0.30 (Met 1), showing a wide range of bond vector dynamics on the ps−ns time scale. Not unexpectedly, there is little correlation between rapid dynamics and the slower exchange process monitored by relaxation dispersion; for example, both Met 1 ($S_{axis}^2 = 0.30$) and Met 6 ($S_{axis}^2 = 0.98$) sense the slow-exchange process and yet clearly have very different amplitudes of motion on the faster time scale.

Figure 6 shows dispersion profiles obtained for four of the methionine residues in a complex of calmodulin and a 26-residue peptide comprising the C-terminal region from petunia glutamate

decarboxylase.[27] The dispersion profiles are flat, indicating that exchange processes with time constants on the order of 1 ms are not occurring at these sites. These flat profiles provide an important experimental control, indicating that relaxation dispersion only occurs in the presence of chemical exchange.

In the present applications we have restricted analysis of the relaxation dispersion profiles to those involving methionine residues. For all other methyl-containing amino acids the large one-bond $^{13}C-^{13}C$ scalar couplings in uniformly ^{13}C-labeled proteins results in efficient magnetization transfer among carbons in the coupled ^{13}C spin network of the side chain. This significantly complicates analysis of exchange since in this case dispersion profiles depend on several factors, including the number of carbons in the side chain, the efficacy of transfer between carbons for a given field strength, ν_{CPMG}, and the relaxation rates of the carbon spins that participate in magnetization transfer. It is possible, however, to prepare proteins that are specifically labeled with ^{13}C at methyl sites, thereby avoiding the problems described above. For example, building on the work of Rosen et al.,[52] Wand and co-workers showed that proteins expressed in *Escherichia coli* with $^{13}C_{methyl}$-pyruvate as the sole carbon source are labeled with ^{13}C at Ala, Val, Leu, and Ile ($C^{\gamma 2}$) methyl positions.[53] In an alternative approach, Gardner and co-workers[54,55] have demonstrated that the methyl groups of Leu and Val residues in proteins expressed using glucose as the carbon source can be labeled by the addition of isovalerate approximately 1 h prior to protein induction, while the Ile C^{δ} position can be labeled using the substrate α-ketobutyrate. Following along the lines of this work, Hajduk et al. have established that the use of $^{13}C_{methyl}$-isovalerate and $^{13}C_{methyl}$-α-ketobutyrate as precursors results in the expected labeling of Val, Leu, and Ile (C^{δ}) methyl groups with ^{13}C and have presented a synthetic strategy for the cost-efficient production of these substrates.[56] Thus, well established methodology is available for labeling proteins selectively at ^{13}C methyl positions, facilitating measurement of dispersion profiles at a large number of methyl-containing side chains using the experiment presented in Figure 1. Indeed we have recently produced a ^{13}C-methyl-labeled sample of L99A using pyruvate as the carbon source

(52) Rosen, M. K.; Gardner, K. H.; Willis, R. C.; Parris, W. E.; Pawson, T.; Kay, L. E. *J. Mol. Biol.* **1996**, *263*, 627−636.

(53) Lee, A. L.; Urbauer, J. L.; Wand, A. J. *J. Biomol. NMR* **1997**, *9*, 437−440.

(54) Gardner, K. H.; Kay, L. E. *J. Am. Chem. Soc.* **1997**, *119*, 7599−7600.

(55) Goto, N. K.; Gardner, K. H.; Mueller, G. A.; Willis, R. C.; Kay, L. E. *J. Biomol. NMR* **1999**, *13*, 369−374.

(56) Hajduk, P. J.; Augeri, D. J.; Mack, J.; Mendoza, R.; Yang, J. G.; Betz, S. F.; Fesik, S. W. *J. Am. Chem. Soc.* **2000**, *122*, 7898−7904.

and are currently recording dispersion curves of all Ala, Val, Leu, and Ile methyls in the protein using the experimental scheme presented in this paper.

As a final note, it is of interest to consider whether other methyl-labeling strategies might be of use in the study of slow dynamic processes. Torchia and co-workers have expressed proteins with protonated 3-^{13}C-pyruvate and D_2O and measured the excess contribution to carbon relaxation of $^{13}CHD_2$ methyl isotopomers arising from chemical exchange.[18] The important advantage in using this approach is that the ^{13}C relaxation rate is significantly reduced relative to fully protonated methyls, providing a very sensitive probe to chemical exchange even in cases where such contributions are small. In addition, relaxation effects from external protons are minimized. However, at least one disadvantage is introduced by deuteration that we have not yet been able to eliminate. As we have discussed previously,[19] the substantial one-bond $^{13}C-^2H$ scalar coupling and the finite relaxation time of the deuteron leads to a contribution to the effective ^{13}C relaxation rate. With this in mind Torchia and co-workers used a minimum carbon pulse separation of 2 ms, corresponding to ν_{CPMG} values greater than approximately 250 Hz. The variation of R_2^{eff} with ν_{CPMG} for $\nu_{CPMG} < 250$ Hz can often be critical for distinguishing between fast and intermediate/slow time-scale exchange regimes and hence for the accurate quantification of the microscopic exchange parameters. In principle, lower ν_{CPMG} fields can be employed if ^2H decoupling is applied in conjunction with the CPMG-train. Unfortunately, in the experiments that we have performed to date the application of ^{13}C refocusing pulses during ^2H decoupling interferes with the decoupling process itself, leading to a modulation of cross-peak intensities as a function of ν_{CPMG} that is not related to exchange. We are currently attempting to understand this process and to develop ^2H decoupling protocols where this deleterious effect is eliminated. Other disadvantages associated with deuteration include the loss of signal from the production of isotopomers other than $^{13}CHD_2$ during protein expression and the extra peaks in spectra arising from methyls of the type CH_3,[18] in particular.

In summary, a method has been described for the quantitation of slow exchange processes at side-chain methyl positions in proteins. A detailed analysis of the evolution of magnetization during the experiment establishes that cross-correlated spin relaxation and scalar coupling do not interfere with the extraction of accurate exchange parameters. The methyl experiment reported herein and the recently described approach for measuring exchange at side-chain NH_2 groups in proteins allow slow processes to be monitored with a significant number of side-chain probes. Ultimately, results from these experiments applied to a large number of systems should increase our understanding of the role of dynamics in conferring specificity and affinity in molecular recognition processes and in defining the pathway of entry and exit of ligands in binding events.

Appendix I

In what follows the matrix representations of $\tilde{Z}$, $\tilde{J}$, $\tilde{\Gamma}_I$, $\tilde{\Gamma}_E$, and $\tilde{P}\tilde{\Gamma}_E\tilde{P}^{-1}$ in the operator basis, $\vec{V}$, eq 3, are given.

$$i\tilde{Z} = i\omega_C\tilde{E} \qquad (AI.1)$$

where $\tilde{E}$ is the 6×6 identity matrix and ω_C is the resonance frequency of the ^{13}C methyl spin.

$$i\tilde{J} = i\pi J_{CH}\begin{vmatrix} 0 & \sqrt{3} & 0 & 0 & 0 & 0 \\ \sqrt{3} & 0 & 2 & 0 & 0 & 0 \\ 0 & 2 & 0 & \sqrt{3} & 0 & 0 \\ 0 & 0 & \sqrt{3} & 0 & 0 & 0 \\ 0 & 0 & 0 & 0 & 0 & 1 \\ 0 & 0 & 0 & 0 & 1 & 0 \end{vmatrix} \qquad (AI.2)$$

where J_{CH} is the one-bond $^1H-^{13}C$ scalar coupling constant.

$$\tilde{\Gamma}_I^{DD} = K^{DD}\begin{vmatrix} 1/2 & 0 & 1/\sqrt{3} & 0 & 0 & 0 \\ 0 & 7/6 & 0 & 1/\sqrt{3} & 0 & 0 \\ 1/\sqrt{3} & 0 & 7/6 & 0 & 0 & 0 \\ 0 & 1/\sqrt{3} & 0 & 1/2 & 0 & 0 \\ 0 & 0 & 0 & 0 & 1/6 & 0 \\ 0 & 0 & 0 & 0 & 0 & 1/6 \end{vmatrix},$$

$$K^{DD} = \frac{6\hbar^2 \gamma_H^2 \gamma_C^2}{r_{HC}^6}J^{DD}(0) \quad (AI.3)$$

where $\tilde{\Gamma}_I^{DD}$ is the contribution to $\tilde{\Gamma}_I$ from $^1H-^{13}C$ dipolar interactions, including cross-correlation effects, γ_i is the gyromagnetic ratio of spin i, r_{HC} is the distance between one-bond coupled $^1H-^{13}C$ spins and

$$J^{DD}(0) = \frac{1}{5} S_{axis}^2\{P_2(\cos\theta_{axis,CH})\}^2 \tau_r \quad (AI.3.1)$$

where the same notation as in eq 1 is used. Note that contributions from fast local motions, second term on the right-hand side of eq 1 are neglected. In this approximation, dipolar interactions between pairs of methyl protons do not give rise to spectral densities at zero frequency.

$$\tilde{\Gamma}_I^{CSA} = K^{CSA}\tilde{E}, \ K^{CSA} = \frac{4}{9}\omega_C^2(\sigma_{||} - \sigma_{\perp})^2 J^{CSA}(0) \quad (AI.4)$$

where $(\sigma_{||} - \sigma_{\perp})$ is the difference between parallel and perpendicular components of the assumed axially symmetric ^{13}C chemical shift tensor and $J^{CSA}(0) = 1/5 \ S_{axis}^2 \tau_r$.

$$\tilde{\Gamma}_I^{DD,CSA} = K^{DD,CSA}\begin{vmatrix} 0 & \sqrt{3} & 0 & 0 & 0 & 0 \\ \sqrt{3} & 0 & 2 & 0 & 0 & 0 \\ 0 & 2 & 0 & \sqrt{3} & 0 & 0 \\ 0 & 0 & \sqrt{3} & 0 & 0 & 0 \\ 0 & 0 & 0 & 0 & 0 & 1 \\ 0 & 0 & 0 & 0 & 1 & 0 \end{vmatrix}$$

$$K^{DD,CSA} = -\frac{4}{3}\frac{\hbar\gamma_H\gamma_C}{r_{HC}^3}\omega_C(\sigma_{||} - \sigma_{\perp})J^{DD,CSA}(0) \quad (AI.5)$$

where

$$J^{\text{DD,CSA}}(0) = \frac{1}{5} S_{\text{axis}}^2 \, P_2(\cos\theta_{\text{axis,CH}})\tau_{\text{r}}$$

$$\tilde{\Gamma}_E = K^E \begin{vmatrix} 0 & 0 & 0 & 0 & 0 & 0 \\ 0 & 1 & 0 & 0 & 0 & 0 \\ 0 & 0 & 2 & 0 & -\sqrt{2} & 0 \\ 0 & 0 & 0 & 3 & 0 & -\sqrt{6} \\ 0 & 0 & -\sqrt{2} & 0 & 1 & 0 \\ 0 & 0 & 0 & -\sqrt{6} & 0 & 4 \end{vmatrix},$$

$$K^E = \frac{1}{2} \frac{\hbar^2 \gamma_{\text{H}}^4}{r_{\text{eff,HH}^E}^6} J^E(0) \quad \text{(AI.6)}$$

where $r_{\text{eff,HH}^E}$ is the effective distance between the external proton spin, H^E, and a methyl proton spin and $J^E(0) = 1/5S_{\text{axis}}^2 \tau_{\text{r}}$. This result is obtained by neglecting contributions from fast local motions (second term on the right-hand side of eq 1) so that auto- and cross-correlated spectral density terms are the same. Note that cross-correlation effects give rise to the off-diagonal elements in the relaxation matrix of eq AI.6. The complete matrix, $\tilde{\Gamma}_E$, can be obtained by summation of the factors K^E over all protons, H^E, in the vicinity of the methyl group.

$$\frac{1}{2}(\tilde{\Gamma}_E + \tilde{P}\tilde{\Gamma}_E\tilde{P}^{-1}) =$$

$$\frac{3}{2} K^E \begin{vmatrix} 1 & 0 & 0 & 0 & \sqrt{\frac{2}{3}} & 0 \\ 0 & 1 & 0 & 0 & 0 & \sqrt{\frac{2}{9}} \\ 0 & 0 & 1 & 0 & -\sqrt{\frac{2}{9}} & 0 \\ 0 & 0 & 0 & 1 & 0 & -\sqrt{\frac{2}{3}} \\ \sqrt{\frac{2}{3}} & 0 & -\sqrt{\frac{2}{9}} & 0 & \frac{5}{3} & 0 \\ 0 & \sqrt{\frac{2}{9}} & 0 & -\sqrt{\frac{2}{3}} & 0 & \frac{5}{3} \end{vmatrix}$$

(AI.7)

Appendix II

The commutativity of $\tilde{\Gamma}_I$ and $\tilde{J}$ in an AX_3 spin system (in the macromolecular limit) can be established by considering the commutation properties of the relevant Hamiltonians without resorting to an explicit calculation of the matrices in a specific operator basis. Consider a scalar coupling Hamiltonian, H_J, and the component of the relaxation Hamiltonian that gives rise to zero-frequency spectral densities, $H_\Gamma(t)$ (e.g., for a proton–carbon dipolar interaction $H_\Gamma(t) = f(t)C_ZH_{Z,1}$ where $f(t)$ contains the interaction constant and the time-modulated spatial part of the interaction). For the pair of (generally distinct) $H_\Gamma(t)$ and $H'_\Gamma(t + \tau)$ satisfying the following conditions

$$[H_J, H_\Gamma(t)] = 0 \quad \text{(AII.1)}$$

$$[H_J, H'_\Gamma(t + \tau)] = 0$$

the corresponding superoperators obey the relationship

$$\hat{\hat{H}}_J\hat{\hat{H}}_\Gamma(t)\hat{\hat{H}}'_\Gamma(t + \tau) = \hat{\hat{H}}_\Gamma(t)\hat{\hat{H}}'_\Gamma(t + \tau)\hat{\hat{H}}_J \quad \text{(AII.2)}$$

To verify eq AII.2 consider the action of $\hat{\hat{H}}_J\hat{\hat{H}}_\Gamma(t)\hat{\hat{H}}'_\Gamma(t + \tau)$ on the operator O_i.

$$\hat{\hat{H}}_J\hat{\hat{H}}_\Gamma(t)\hat{\hat{H}}'_\Gamma(t + \tau)O_i = [H_J,[H_\Gamma(t),[H'_\Gamma(t + \tau),O_i]]] =$$

$$[H_\Gamma(t),[H_J,[H'_\Gamma(t + \tau),O_i]]] - [[H'_\Gamma(t + \tau),O_i],[H_J,H_\Gamma(t)]] =$$

$$[H_\Gamma(t),[H'_\Gamma(t + \tau),[H_J,O_i]]] - [H_\Gamma(t),[O_i,[H'_\Gamma(t + \tau),H_J]]] =$$

$$\hat{\hat{H}}_\Gamma(t)\hat{\hat{H}}'_\Gamma(t + \tau)\hat{\hat{H}}_JO_i \quad \text{(AII.3)}$$

where we have made use of the identity, $[X,[Y,Z]] = [Y,[X,Z]] - [Z,[X,Y]]$, and the conditions given in eq AII.1. Equation AII.2 can be now evaluated in the spin operator basis O_k using the resolution of identity, $E = \sum_j|O_j\rangle\langle O_j|$, leading to:

$$\sum_j \langle O_k|\hat{\hat{H}}_J|O_j\rangle\langle O_j|\hat{\hat{H}}_\Gamma(t)\hat{\hat{H}}'_\Gamma(t + \tau)|O_l\rangle =$$

$$\sum_j \langle O_k\hat{\hat{H}}_\Gamma(t)\hat{\hat{H}}'_\Gamma(t + \tau)|O_j\rangle\langle O_j|\hat{\hat{H}}_J|O_l\rangle \quad \text{(AII.4)}$$

This result contains the J-coupling matrix elements, $\tilde{J}_{pq} = \langle O_p|\hat{\hat{H}}_J|O_q\rangle$. Calculating the time-average on the left- and right-hand sides of eq AII.4 and evaluating the spectral densities at zero frequency following the guidelines of standard Redfield theory[57] one obtains the relaxation matrix elements:

$$\tilde{\Gamma}_{pq} = \int_0^\infty \overline{\langle O_p|\hat{\hat{H}}_\Gamma(t)\hat{\hat{H}}'_\Gamma(t + \tau)|O_q\rangle}d\tau \quad \text{(AII.5)}$$

Therefore, eq AII.4 is equivalent to:

$$\sum_j \tilde{J}_{kj}\tilde{\Gamma}_{jl} - \sum_j \tilde{\Gamma}_{kj}\tilde{J}_{jl} = 0 \quad \text{(AII.6)}$$

or

$$[\tilde{J},\tilde{\Gamma}] = 0 \quad \text{(AII.7)}$$

which is the desired commutativity property for the two matrices.

Thus, to establish the property eq AII.6 it is sufficient to verify the commutativity of the relevant Hamiltonians, eq AII.1, which is usually straightforward. Along these lines it can be demonstrated that $[\tilde{J},\tilde{\Gamma}_I] = 0$. However, for relaxation via dipolar interactions with external protons the condition eq AII.1 is not fulfilled and, hence, $[\tilde{J},\tilde{\Gamma}_E] \neq 0$.

JA004179P

(57) Abragam, A. *Principles of Nuclear Magnetism*; Clarendon Press: Oxford, 1961.

(58) Levitt, M.; Freeman, R. *J. Magn. Reson.* **1978**, *33*, 473−476.

(59) Geen, H.; Freeman, R. *J. Magn. Reson.* **1991**, *93*, 93−141.

(60) Shaka, A. J.; Keeler, J.; Frenkiel, T.; Freeman, R. *J. Magn. Reson.* **1983**, *52*, 335−338.

(61) Marion, D.; Ikura, M.; Tschudin, R.; Bax, A. *J. Magn. Reson.* **1989**, *85*, 393−399.